Nanoscale Advances

ROYAL SOCIETY OF CHEMISTRY

PAPER

Cite this: *Nanoscale Adv.*, 2024, **6**, 233

Carbon sphere doped CdS quantum dots served as a dye degrader and their bactericidal behavior analysed with *in silico* molecular docking analysis

Muhammad Ikram, *[a] Misbah Naz,[b] Ali Haider, *[c] Iram Shahzadi,[d] Hafiz Umar Mehboob,[b] Muhammad Ahsaan Bari,[a] Anwar Ul-Hamid,[e] Mohammed M. Algaradah[f] and Murefah mana Al-Anazy[g]

Received 1st August 2023
Accepted 15th November 2023

DOI: 10.1039/d3na00579h

rsc.li/nanoscale-advances

We have employed a co-precipitation method to synthesize different concentrations of carbon spheres (CSs) doped with cadmium sulfide (CdS) quantum dots (QDs) for catalytic reduction and antibacterial applications. Various morphological and structural characterization techniques were used to comprehensively analyze the CS effect on CdS QDs. The catalytic reduction efficiency of CS-doped CdS QDs was evaluated using rhodamine B dye. The antibacterial efficacy was also assessed against the pathogenic microorganism *Escherichia coli* (*E. coli*), and substantial destruction in the inhibitory zone was measured. Finally, the synthesized CS-doped CdS QDs demonstrated favorable results for catalytic reduction and antibacterial applications. Computational studies verified the suppressive impact of these formed QDs on DNA gyrase and β-lactamase of *E. coli*.

1. Introduction

Water is an indispensable component of living things and plays an integral part in the growth of industry and economic activity across the globe. As drinkable water is becoming polluted worldwide, exploring different water purification methods and developing new ones is more critical than ever. Because of their potentially harmful effects, organic contaminants found in wastewater from industrial and agricultural processes pose a significant risk to aquatic life and other forms of life. Wastewater from industries producing leather, pulp, polymer, fabric, pharmaceuticals, and pesticides contains many organic toxins, especially dyes, which pollute water and damage life on Earth.[1] Approximately ten to fifteen percent of these dyes are released directly into the environment and aquatic bodies.[2] The removal of dyes has been accomplished using the processes of membrane filtering,[3] ozonation,[4] catalytic reduction,[5,6] and adsorption[7] in a variety of different ways. Catalytic reduction is believed to be good for the environment, energy efficient, economically viable, and very effective in totally mineralizing and oxidizing dangerous organics.[8,9]

On the other hand, bovine mastitis is the disease that affects cows most frequently; it is the cause of alterations in milk quality and quantity, as well as an increase in the number of cullings, which can result in significant financial losses. Mastitis progresses through two stages: the clinical stage as well as the subclinical stage. Clinical mastitis symptoms include soreness, edema, fever, and irregular milk flow. Subclinical mastitis symptoms include an increase in somatic cells, but no other systemic symptoms or observable changes in the milk are present.[10] The severity of clinical mastitis can range anywhere from mild to severe.[11] One of the most common causes of mastitis is *E. coli*, which can also cause toxemia, high fevers, moderate to severe inflammation, and decreased milk production.[12]

To address these challenges, nanotechnology is currently employed in many industries, including medicine, food production, and water purification.[13] In recent years, several types of semiconductors, including CdS, CdSe, ZnSe, CuO, and ZnO, have been manufactured by employing a variety of manufacturing processes.[14–18] The co-precipitation method is uncomplicated, cost-effective, and only requires one step.[19] Cadmium sulfide (CdS) quantum dots (QDs) stand out among the other types of semiconductors because of their unique chemical and physical features.[20] CdS has a large band gap, with an energy of 2.42 eV.[21] CdS QDs have a high dye degradation

[a]*Solar Cell Applications Research Lab, Department of Physics, Government College University Lahore, Lahore, 54000, Punjab, Pakistan. E-mail: dr.muhammadikram@gcu.edu.pk*

[b]*Department of Chemistry, University of Education, Township, Lahore, 54000, Pakistan*

[c]*Department of Clinical Sciences, Faculty of Veterinary and Animal Sciences, Muhammad Nawaz Shareef, University of Agriculture, 66000, Multan, Punjab, Pakistan*

[d]*School of Pharmacy, University of Management and Technology, Lahore 54770, Pakistan*

[e]*Core Research Facilities, King Fahd University of Petroleum & Minerals, Dhahran 31261, Saudi Arabia*

[f]*Chemistry Department, King Khalid Military Academy, Riyadh 11495, Saudi Arabia*

[g]*Department of Chemistry, College of Sciences, Princess Nourah bint Abdulrahman University (PNU), P.O. Box 84428, Riyadh 11671, Saudi Arabia*

efficiency, making them helpful in treating wastewater and the catalytic destruction of dyes.

On the other hand, the production of large CdS QDs gave rise to a reduction in surface area as a result of aggregation as well as an increase in the rate of exciton recombination.[22] To address this challenge, using carbon spheres is deemed advantageous in regulating the morphology and dimensions of QDs. Carbon spheres (CSs) have a large surface area and good electrical conductivity. When used as a dopant to CdS, CS can modify CdS properties and enhance its performance in applications such as photocatalysis and antimicrobial activity.[23] The large surface area of CSs provides a sizeable active site for catalytic reactions, while their good electrical conductivity enhances charge transfer between CdS and target pollutants. CS thermal stability also protects CdS from thermal degradation, and its low toxicity makes it a safer alternative. The characteristics above render CS a potentially favorable substance for implementation as a dopant into CdS for an array of applications.[23,24]

The present study involved the synthesis of CS-doped CdS quantum dots (QDs) using the co-precipitation technique. The current research examined the effects of both undoped and doped specimens on the degradation of RhB and their bactericidal effectiveness against *E. coli*. Furthermore, the impact of dopants on the morphological, optical, structural, and chemical composition of CdS has been investigated and discussed.

2. Experimental details

2.1 Chemicals

Cadmium chloride ($CdCl_2$) was purchased from PRS. Glucose ($C_6H_{12}O_6$), sodium hydroxide (NaOH), ammonia (NH_3), thiourea (CH_4N_2S), sodium borohydride, and rhodamine B were obtained from Sigma-Aldrich. Without further purification, all of the compounds were utilized.

2.2 Synthesis of carbon spheres

The carbonization of glucose by hydrothermal processes resulted in the production of carbon spheres (CSs). Typically, 1 M glucose solution was stirred until it became transparent and clear. Afterward, the colloidal solution was placed into an autoclave with a Teflon seal and heated for 12 hours at 180 °C. The resultant precipitates have been washed with distilled water numerous times before being dried for a whole night at 100 °C.

2.3 Synthesis of CS doped-cadmium sulphide

To prepare cadmium sulphide QDs, 0.2 M $CdCl_2$, and 0.2 M CH_4N_2S solution were mixed under vigorous stirring at 80 °C. After 30 minutes, 1 M NaOH solution was poured dropwise into the above-prepared colloidal solution to sustain the pH ∼ 12. Moreover, precipitate formation began, and a fixed amount of NH_3 was introduced. After this, the solution was continuously stirred for 2 hours under constant heating at 80 °C. The obtained solution has been centrifuged multiple times at 7000 revolutions per minute for 420 seconds and then heated at 140 °C for 12 hours. The synthesis of CdS doped with carbon spheres (CS) at concentrations of 1%, 3%, and 5% has been carried out using a similar methodology (Fig. 1).

2.4 Isolation and identification of MDR *E. coli*

2.4.1 Isolation of *E. coli*

2.4.1.1 Sample collection. Sterile glassware was utilized to directly milk specified lactating cows and collect raw milk samples from diverse farms, veterinary hospitals, markets, and

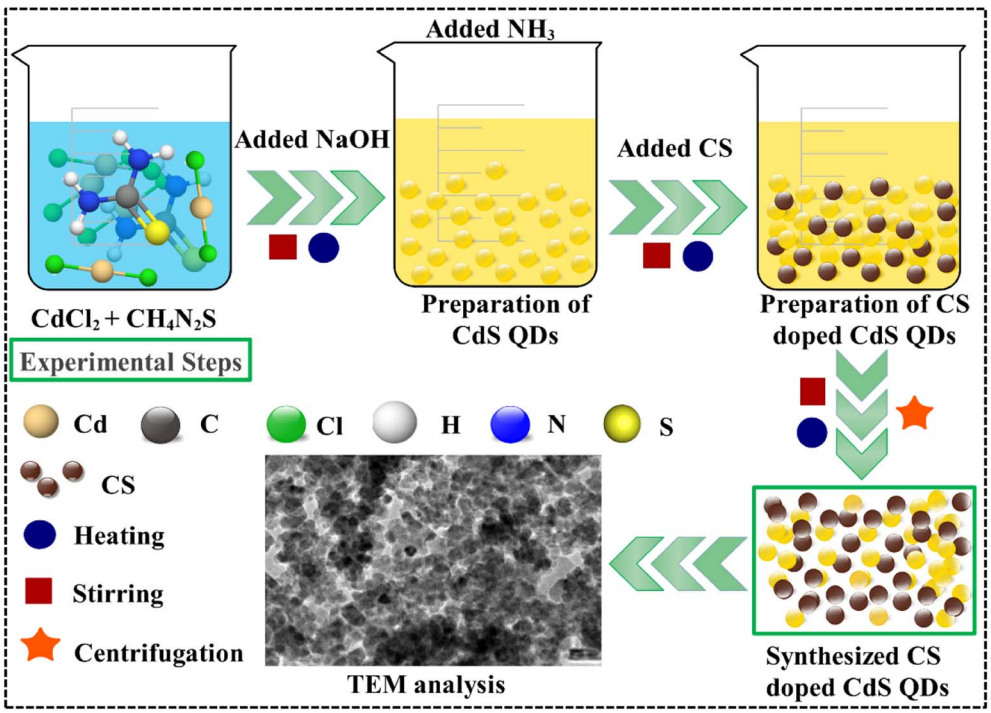

Fig. 1 Preparation of CS doped CdS QDs.

the Punjab province of Pakistan. As soon as it was collected, the raw milk was taken into the laboratory and kept at a temperature of 4 °C. To determine the overall quantity of coliforms that exist in raw milk, MacConkey agar was used. At a temperature of 37 °C, each plate was incubated in an incubator for 48 hours.

2.4.1.2 Identification and characterization of bacterial isolates. To conduct an initial diagnosis of *E. coli*, the morphology of the colony was analyzed through the application of the Gram stain technique. Additionally, a variety of biochemical assays were performed following Bergey's manual of determinative bacteriology.[25]

2.4.2 Antibiotic susceptibility. The antibiotic susceptibility test was performed using the Bauer *et al.*[26] disc diffusion method on Mueller–Hinton agar (MHA) (Oxoid Limited, Basingstoke, UK). The following antibiotics (classes) were used in the experiment to assess whether or not *E. coli* was resistant to certain antibiotics; gentamicin (Gm) 10 μg (aminoglycosides), ciprofloxacin (Cip) 5 μg (quinolones), tetracycline (Te) 30 μg (tetracyclines), ceftriaxone (Cro) 30 μg (cephalosporins), azithromycin (Azm) 15 μg (Macrolides), amoxycillin (A) 30 μg (penicillins), and imipenem (Imi) 10 μg (carbapenem).[27] The turbidity of the *Escherichia coli* cultures following purification has been standardized to 0.5 MacFarland. Subsequently, the sample was dispersed onto MHA, and antibiotic discs were evenly distributed on the inoculated plate surface, maintaining a suitable distance between them to avoid any potential merging of inhibition zones. Following a 24 hour incubation period at 37 °C, the data were analyzed under guidelines established by the Laboratory and Clinical Standard Institute.[28] A bacterium was deemed MDR if it was shown to be resistant to at least three antibiotics.[29]

2.4.3 Antimicrobial activity. Using the agar well diffusion method, 10 typical isolates of multidrug-resistant *E. coli* obtained from mastitic milk were used to assess the *in vitro* antibacterial activity of the produced QDs. MDR *E. coli* was swabbed onto MacConkey agar-coated Petri plates at a concentration of 1.5×10^8 CFU ml^{-1} (0.5 McFarland standard). 6 mm-diameter holes were drilled into the cork using a sterile cork borer. This investigation used pure and CS-doped CdS in different concentrations (0.5 mg/50 μL, 1.0 mg/50 μL). Ciprofloxacin (0.005 mg/50 μL) was utilized as a positive control, while DIW (50 μL) was used as a negative control.[30]

2.4.4 Statistical analysis. The statistical evaluation of the inhibition zone diameters was conducted in SPSS 20 utilizing one-way analysis of variance (ANOVA) to establish the antimicrobial effectiveness concerning the mm of the inhibition zone.[31]

2.4.5 Molecular docking analysis. The targets of the current investigation were *E. coli* enzymes, DNA gyrase (PDB ID: 6KZX)[32] and β-lactamase (PDB ID: 4KZ9, resolution: 1.72)[33] involved in the nucleic acid synthesis and the peptidoglycan pathway, accordingly. Using the corresponding PDB IDs, the Protein Data Bank was queried for 3D structures. Sybyl X-2.0 (ref. 34 and 35) is utilized to predict molecular connections relying on module-built schematic ligand frameworks. The energy was retained by replacing natural ligands in water molecules with polar H atoms. PyMol was utilized to develop a three-dimensional representation of binding interactions.

2.5 Catalytic reduction of rhodamine B

To determine the efficacy of the catalytic reduction of RhB, a fresh 0.1 M solution of RhB and a 0.1 M solution of $NaBH_4$ have been prepared. Initially, a freshly made 400 μL $NaBH_4$ solution was added to a 1.5 mL aqueous solution of RhB. In the second step, 400 μL of the prepared nanocatalyst (pure and doped CdS QDs) was added to the solution before being mixed well. To calculate the rate at which the RhB organic dye deteriorated, the progression of the absorption reaction was monitored with a UV-vis spectrophotometer at room temperature after a predetermined time interval. The effective degradation of the dye was demonstrated by the transformation of RhB into its leuco form when a nanocatalyst was added. The percentage of degradation was calculated as follows:

$$\text{Degradation}\% = \frac{C_0 - C_t}{C_0} \times 100 \quad (1)$$

where C_0 is the initial absorbance and C_t is the concentration at a specific time after the incorporation of materials.

2.5.1 Mechanism. The incorporation of a nanocatalyst as well as a reducing agent is considered a fundamental step that is believed to exert a pivotal influence on the catalytic mechanism. A redox reaction took place during the catalytic reduction, which involved the transfer of electrons (e^-) from the reductant ($NaBH_4$) to the oxidant (RhB). As a direct consequence, the dye began to degrade because of accepting electrons (Fig. 2). Also, RhB degradation with a reducing agent ($NaBH_4$) was evaluated without nanocatalysts; this oxidation–reduction reaction was time-consuming and exceedingly slow. The addition of nanocatalysts into oxidation–reduction reactions boosted the degradation rate, serving as an electron relay and speeding up the electron transfer from the donor (BH_4^-) to the acceptor. Using QDs increases the adsorption of BH_4^- ions and dye molecules, as QDs provide many active sites, encouraging them to react with each other more quickly, ultimately leading to a practical breakdown of the dye.[36]

2.6 Characterization techniques

After being synthesized, CdS and CS-doped CdS QDs were characterized using elemental, structural, and optical

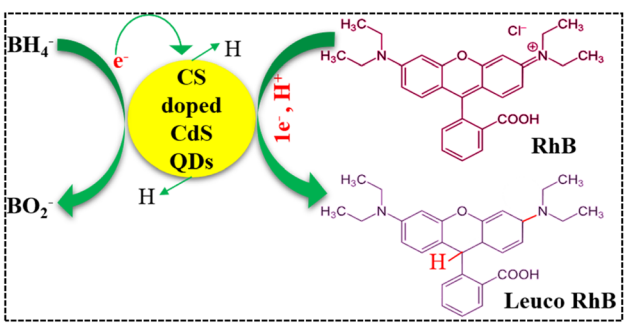

Fig. 2 Possible mechanism for catalytic reduction of the RhB dye.

techniques. Energy-dispersive X-ray spectroscopy (EDS, JEOL-JSM-6460LV) was used for elemental analysis. Powder X-ray diffraction was used to investigate the structural properties. Field emission scanning electron microscopy (JEOL-JSM-6460LV) and high-resolution transmission electron microscopy (JEOL JEM 2100F) were used to assess the surface morphology and the size of the particles. Using ultraviolet-visible spectroscopy, the optical characteristics were analyzed and characterized.

3. Results and discussion

X-ray diffraction has been utilized to analyze the polymorphic structures as well as crystallographic phases of both the as-synthesized CdS as well as the CS-doped CdS QDs (Fig. 3a). The CdS QDs synthesized through the co-precipitation technique displayed the diffraction lines of the (100), (002), (101), (102), (110), (103), and (112) planes at $2\theta = 24.9°$, 26.6°, 28.3°, 36.8°, 43.9°, 48.1°, and 52.1°, which confirms the hexagonal phase of CdS corresponding to JCPDS card no. 01-080-0006. The other two peaks were observed in all samples exhibiting diffraction lines of the (112) and (240) planes at $2\theta = 31.9°$ and 56.9°, which agree with JCPDS card no. 00-015-0086 for cadmium sulfate ($CdSO_4$) and reveals the orthorhombic structure. The peaks indicated that the samples are crystalline, with the most intense diffraction peak attributable to the (002) diffraction plane denoting the preferred formation of CdS crystallites along the [001] direction.[37] Two peaks, exhibiting diffraction lines of the (002) and (101) planes at $2\theta = 24.3°$ and 44.0°, were observed after CS doping,[38] which confirmed the successful doping of CS to CdS QDs. Moreover, when the concentration of CS is increased, the broadening of peaks is observed, and some slight peaks seem to disappear, suggesting the amorphous nature of carbon.[38] The addition of CS does not affect the hexagonal phase in pristine CdS. According to reports, CdS exhibiting a hexagonal crystal structure, excellent crystallinity, and a substantial surface area has demonstrated enhanced catalytic activity and superior stability compared to the pure cubic phases.[39] The enhanced catalytic activity of CdS with a high aspect ratio can be attributed to the confinement of electrons in a specific path, which significantly impacts the optical and electrical characteristics of the catalyst.[40] Using the Debye Scherrer equation, $D = k\lambda/\beta \cos\theta$, the average crystal sizes for CdS and CS-CdS (1%, 3%, and 5%) were determined to be 18.94, 57.93, 60.92 and 85.48 nm, respectively. The crystallite size increases upon varying the CS concentration, which could be attributed to the peak broadness and amorphous nature of CSs. The SAED patterns confirmed the crystallinity of the synthesized pure and doped CdS QDs (Fig. 3b–e). The rings with bright spots in the SAED patterns suggest that the CdS and (1, 3, 5 wt%) CS-doped CdS QDs are polycrystalline.

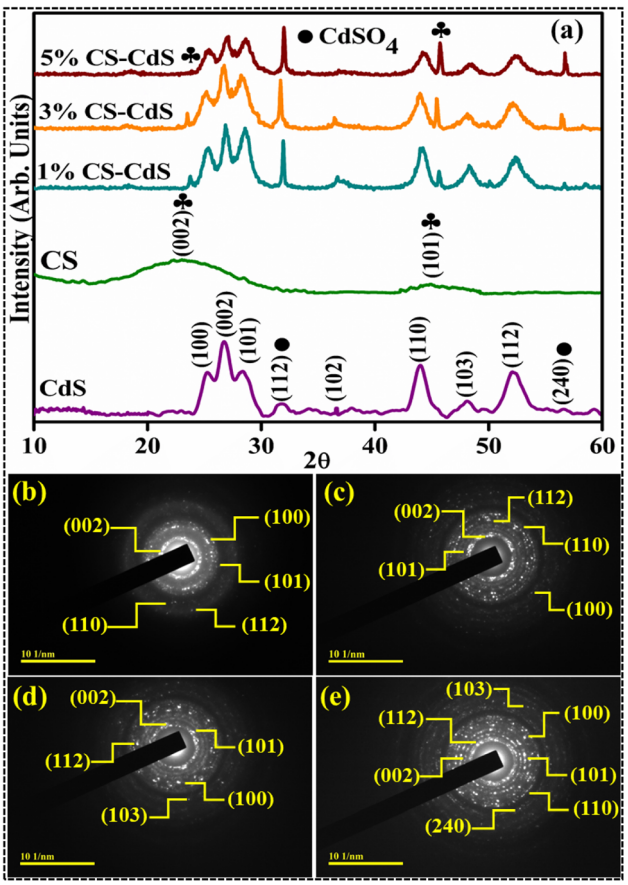

Fig. 3 (a) XRD and (b–e) SAED patterns of CdS, 1% CS doped CdS, 3% CS doped CdS, and 5% CS doped CdS QDs, respectively.

The surface morphology of unmodified and CS-doped CdS quantum dots was investigated using the SEM technique, as depicted in Fig. 4. CdS exhibited agglomerated, non-uniform chunks containing undissolved particles of moderate size (Fig. 4a). With the addition of CSs; the particles appear to have a more random attachment, corresponding to their reduced size (Fig. 4b and c). When the amount of doping was increased, a morphology identical to a sphere emerged, and particles started appearing on the surface of chunks (Fig. 4d).

EDS analysis confirmed the elemental composition and purity of the prepared nanocatalyst, as shown in Fig. 5a–d. Substantial Cd and S peaks were seen, ensuring that the preparation of CdS was successful. The sodium (Na) peak in the samples can be attributed to utilizing NaOH during synthesis to maintain pH. In contrast, the gold (Au) peaks can be traced back to the coating applied on the samples to mitigate the charging effects. Using a brass sample holder in the EDS analysis procedure could have resulted in certain impurities and the manifestation of insignificant peaks of Cs, In, O, and Zn. In addition, the chlorine (Cl) peak was seen as a result of the precursor utilized throughout the synthesis process.

In addition, an EDS mapping analysis was conducted on the highly doped specimen in its as-prepared form to investigate the elemental distribution and assess any potential interfacial contact, as depicted in Fig. 5e–j. The highly doped samples showed a dispersion of six elements (Cd, S, Na, Cs, Cl, and O). As discussed earlier, the elements Na, Cs, S, and Cl were attributed to the utilization of precursor material during the synthesis process, contamination, and the sample holder utilized for EDS analysis.

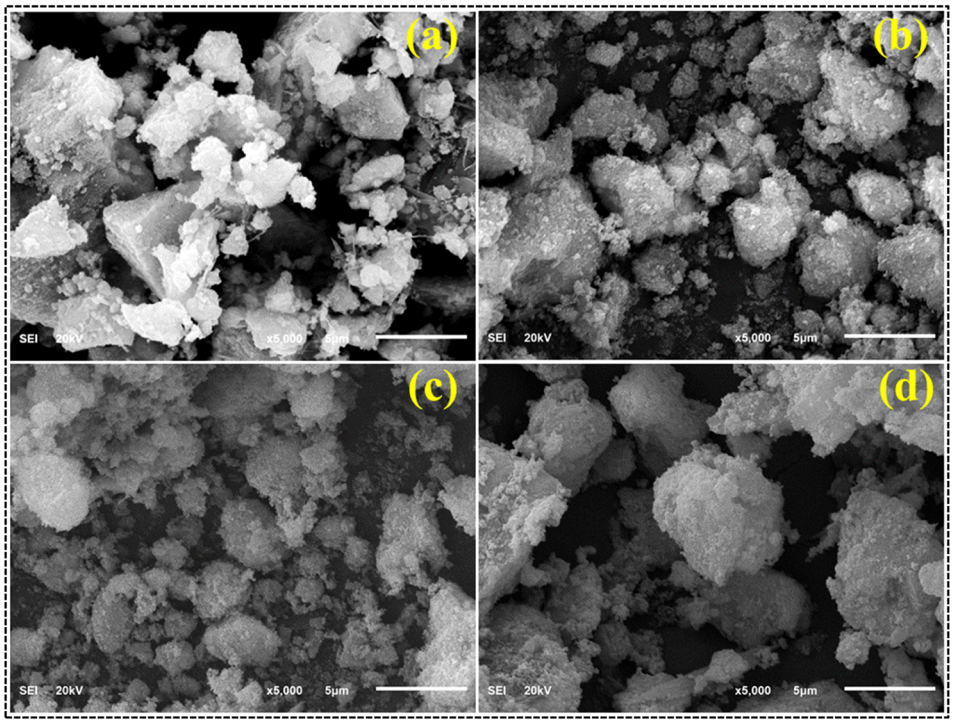

Fig. 4 FESEM images of (a) CdS, (b) 1% CS doped CdS, (c) 3% CS doped CdS and (d) 5% CS doped CdS QDs.

Using TEM micrographs, the morphological examination of the samples was investigated (Fig. 6a–d). According to TEM analysis, CdS (Fig. 6a) exhibited a spheroidal shape with significant clustering. Upon the incorporation of 1% CSs, the particles seemed to agglomerate and take on a spherical shape (Fig. 6b). Particle size decreases, and dense clusters form when the doping concentration increases to 3% (Fig. 6c). Tiny particles can sometimes be found piled on top of one another. The spherical shape of the particles upon 5% CS doping verifies the accomplishment of CS doping (Fig. 6d). Agglomeration occurs when forces of attraction are dominant between the particles. Particles build a network of quantum dots (QDs) by weakly adhering to one another through overlapping QDs, a manifestation of Brownian agglomeration.[41,42] Using the ImageJ software, the particle size was determined to be 12.94 nm for pure CdS QDs, 9.16 nm for CdS QDs with 1% CS doping, 7.42 nm for CdS QDs with 3% CS doping, and 6.89 nm for CdS QDs with 5% CS doping. Moreover, the decrease in particle size with increasing doping concentration may result in an enhanced surface area of the particle, which ultimately results in dye degradation as well as antimicrobial activity.

Furthermore, the measurement of the interlayer spacing of the CdS quantum dots yielded a value of 0.339 nm, which is consistent with the X-ray diffraction measurement obtained from the crystallographic (002) plane, as depicted in Fig. 7a. The observed trend in the present study indicates a gradual reduction in the d spacing, with values ranging from 0.330 to 0.326 nm, in response to an increase in the doping concentration of CSs (Fig. 7b–d).

To analyze the optical properties, the prepared samples, including CdS and CS-doped CdS QDs, their UV-vis absorption spectra were examined, as shown in Fig. 8a. At a wavelength of 505 nm, the edge of the absorption band for CdS was designated by the transition of an electron from the 4d state of Cd to the 3p state of S, respectively.[43,44] Following the introduction of doping, a blueshift has been observed in the absorption spectra, accompanied by slightly high band gap energy (E_g) values, manifested as the quantum confinement effect.[45,46] Moreover, bandgap energy (E_g) was calculated using the Tauc equation (Fig. 8b). The E_g was found to be 2.42 eV for CdS, 2.51 eV for 1 wt% CS-doped CdS QDs, 2.53 eV for 3% CS-doped CdS, and 2.56 eV for 5 wt% CS-doped CdS.

The current investigation assessed the potential application of both pure and doped CdS QDs through catalytic degradation of RhB dye in the presence of $NaBH_4$, as depicted in Fig. 9. Since dye sludge is commonly released at different pH levels, the catalytic performance of the synthesized nanocatalysts is assessed at several pH values 4 (acidic), 7 (neutral), and 12 (basic). The acidic pH was maintained at 4 using H_2SO_4, while the basic pH was adjusted to 12 by incorporating NaOH. Fig. 9 shows that $NaBH_4$ in the absence of a nanocatalyst shows a minimal degradation efficiency of 14.28% in acidic, 28.57% in basic, and 11.11% in neutral media. The breakdown of RhB involves the transfer of electrons from $NaBH_4$ to the dye. Still, the effectiveness of the reduction was constrained by the significant difference in redox potential between RhB and BH_4^-.[47] Upon the incorporation of pure and (1%, 3%, and 5%) CS doped CdS QDs into a mixture of the dye and $NaBH_4$, the maximum degradation efficiency was observed to be 84.57, 84.71, 85.28, and 89% in acidic, 36.71, 37.28, 66.28, and 73.14% in basic and 27.55, 42.22, 52.55, and 69% in neutral media. The nanocatalyst in pure and doped CdS QDs served as a bridge

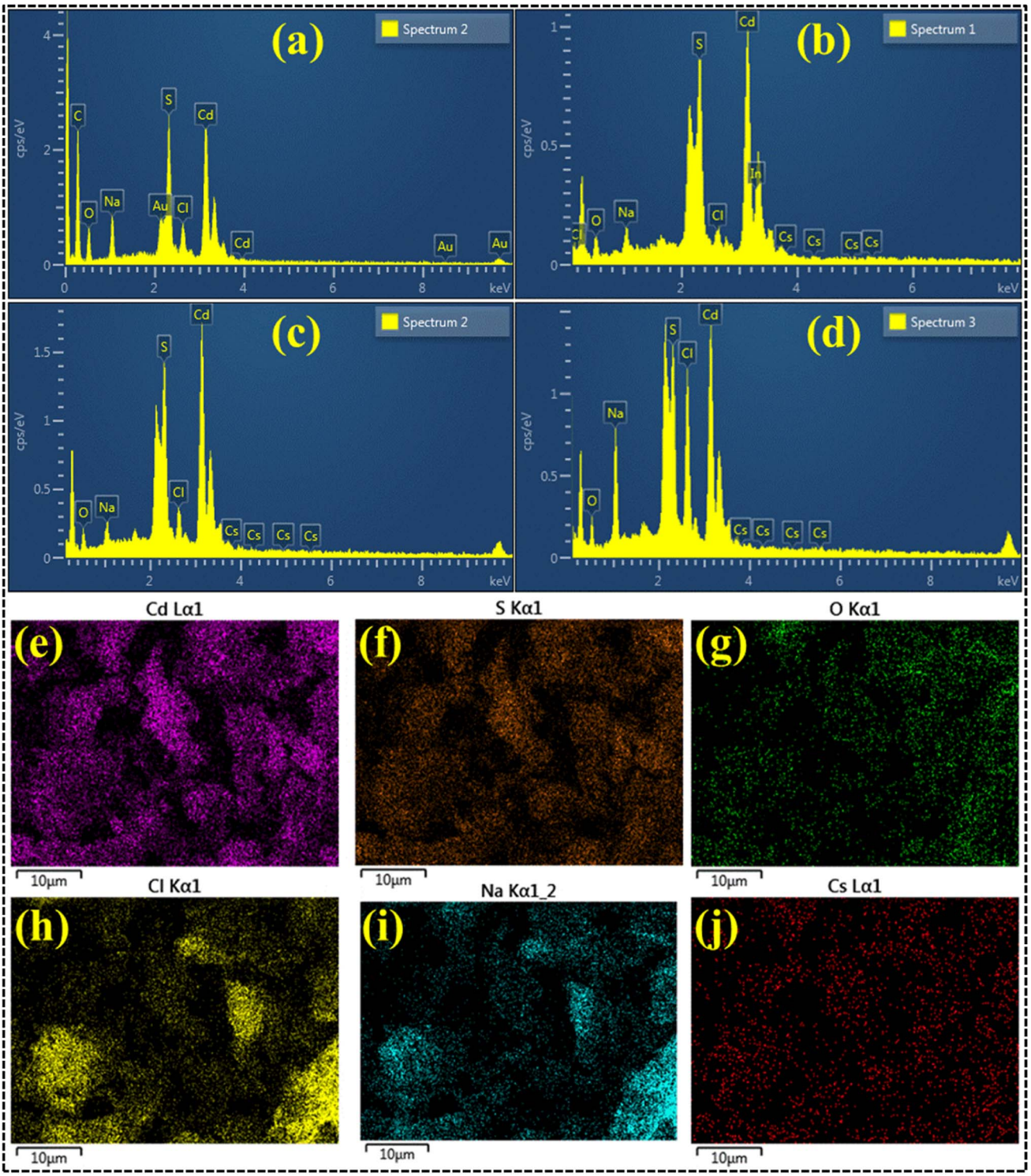

Fig. 5 EDS analysis of (a) CdS, (b) 1% CS doped CdS, (c) 3% CS doped CdS and (d) 5% CS doped CdS; (e–j) elemental mapping of 5% CS doped CdS QDs.

between the high redox potential and the catalyzed degradation of the dye molecules by relaying the electrons absorbed from BH_4^- ions. The RhB molecules could diffuse *via* the pores and channels in the pure and doped CdS QDs, increasing the interactions between the nanocatalyst, BH_4^- and RhB.[48] RhB degraded more effectively in acidic media than in other media, related to the higher generation of H^+ ions available for absorption on the surface of the QDs. In a basic medium (NaOH), as the number of hydroxyl groups increases, reduced products are oxidized, which lowers catalytic effectiveness. The

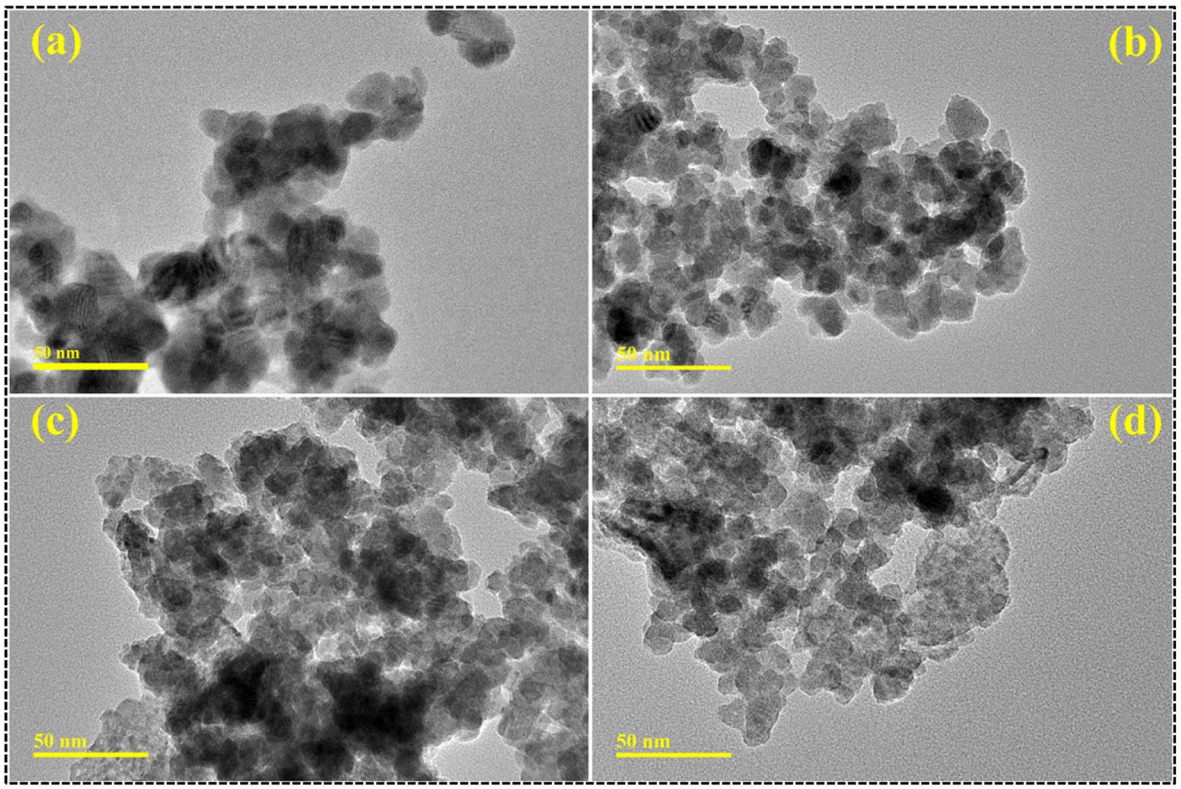

Fig. 6 TEM micrographs of (a) CdS, (b) 1% CS doped CdS, (c) 3% CS doped CdS and (d) 5% CS doped CdS QDs.

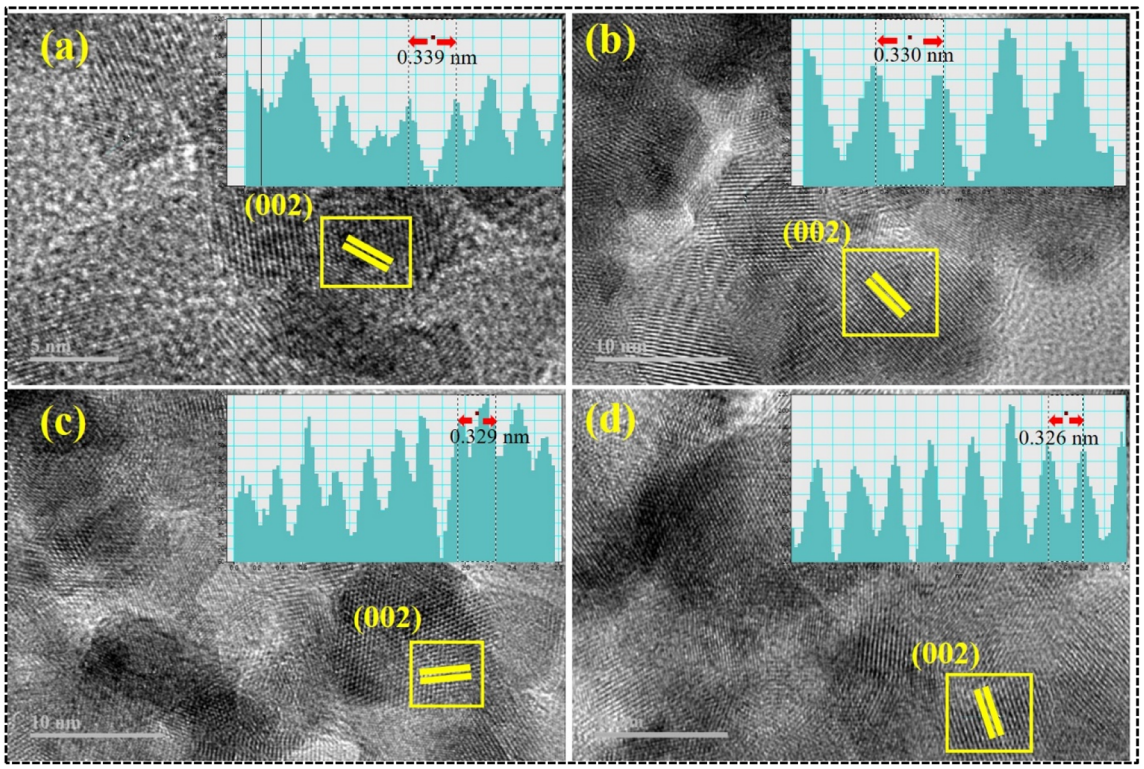

Fig. 7 Interlayer spacing of (a) CdS, (b) 1% CS doped CdS, (c) 3% CS doped CdS and (d) 5% CS doped CdS QDs.

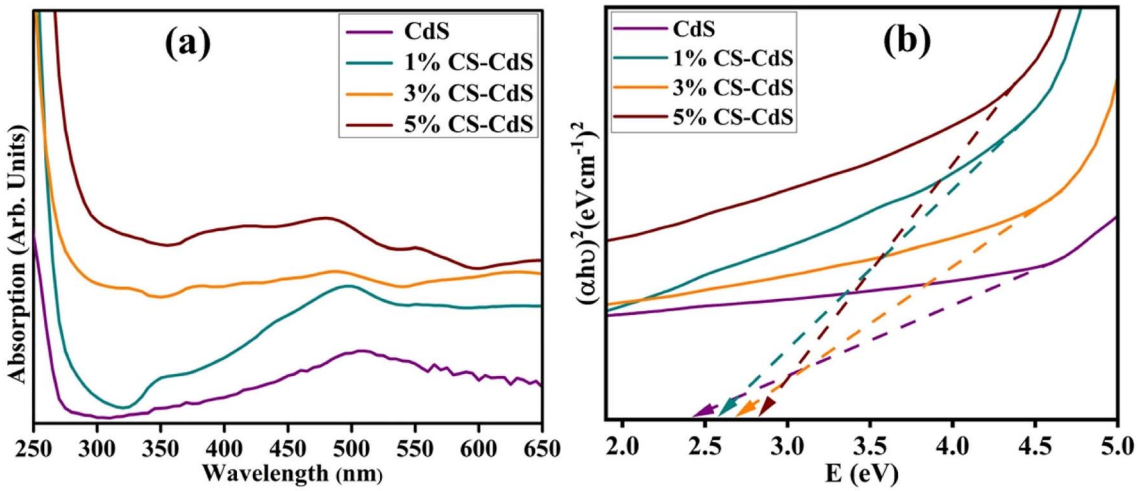

Fig. 8 (a) Absorption spectra and (b) E_g by using the Tauc plot of pristine and CS doped CdS QDs.

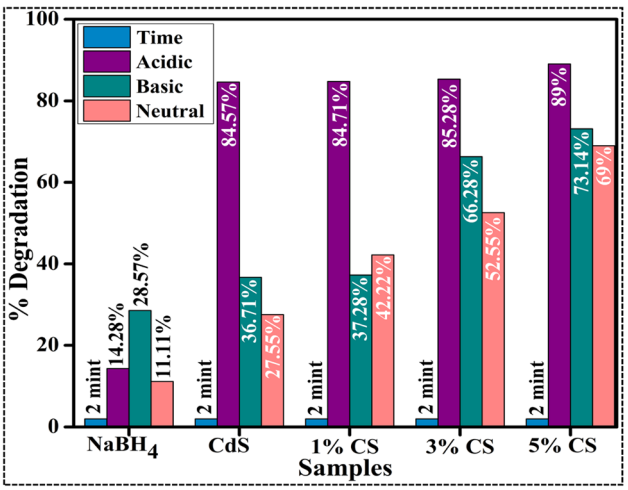

Fig. 9 Catalytic reduction of RhB dye using the prepared nanocatalyst.

surface area, shape, and crystallinity of QDs affect catalytic activity.[49,50] Catalysts with more significant surface area are frequently used since they provide more active sites and exhibit superior catalytic effectiveness.[51,52] As such, the increase in catalytic effectiveness in this study is attributable to the morphological alteration (quantum dots), which increased the surface-to-volume ratio and offered more surface area for the reaction to occur on account of a decrease in particle size. Moreover, the comparison of the present work with the literature is presented in Table 1.

In addition, from the above findings, an effective degradation was observed in an acidic medium; therefore, a stability and reusability test was carried out in an acidic medium. To conduct the stability test, the samples were stored for 72 hours and examined after every 24 hours. Almost minimal discernible change was observed in the nanocatalyst stability even after 72 hours (Fig. 10b). Moreover, to make the nanocatalysts reusable, they were centrifuged, washed, and dried before the next experiment. As shown in Fig. 10b, the catalytic reduction performance of the RhB dye was not significantly impacted even after being subjected to five cycles. In each run, it demonstrated excellent performance as well as stability. Based on these results, the synthesized nanocatalyst has a high stability level and can be reused for the catalytic reduction of organic contaminants. To get a deeper comprehension of the degradation process, trapping studies were conducted to examine the active species involved in the degradation of RhB. As seen in Fig. 10c, degradation of RhB exhibits no variation in the presence of 1, 4-benzoquinone (BQ, quencher of $^{\bullet}O_2^-$), which implies that $^{\bullet}O_2^-$ is not the predominant reactive species for the degradation process. The inclusion of isopropanol (IPA), known to quench hydroxyl radicals ($^{\bullet}OH$), resulted in the deceleration of degradation of RhB. In contrast, adding ethylenediaminetetraacetic acid disodium (EDTA-2Na) quenches H^+, resulting in total suppression of degradation. This observation

Table 1 Comparison table for the degradation of dyes

Nanocatalysts	Synthesis approach	Dye	Outcomes	References
CdS/ZnO	Hydrothermal and photochemical	RhB	85% in 8 hours	53
CdS nanorods	Solvothermal method	RhB	88.4% in 2 hours	54
CdS/MoS_2	Solvothermal method	RhB	84% in 2 hours	55
Bi/CdS/TiO_2 nanotubes	Successive ionic layer adsorption and reaction (SILAR) method	RhB	85.41% in 2 hours	56
CdS/TiO_2	Chemical precipitation technique	AB-29	84%	57
CS/CdS	Co precipitation	RhB	89% in 2 minutes	Present work

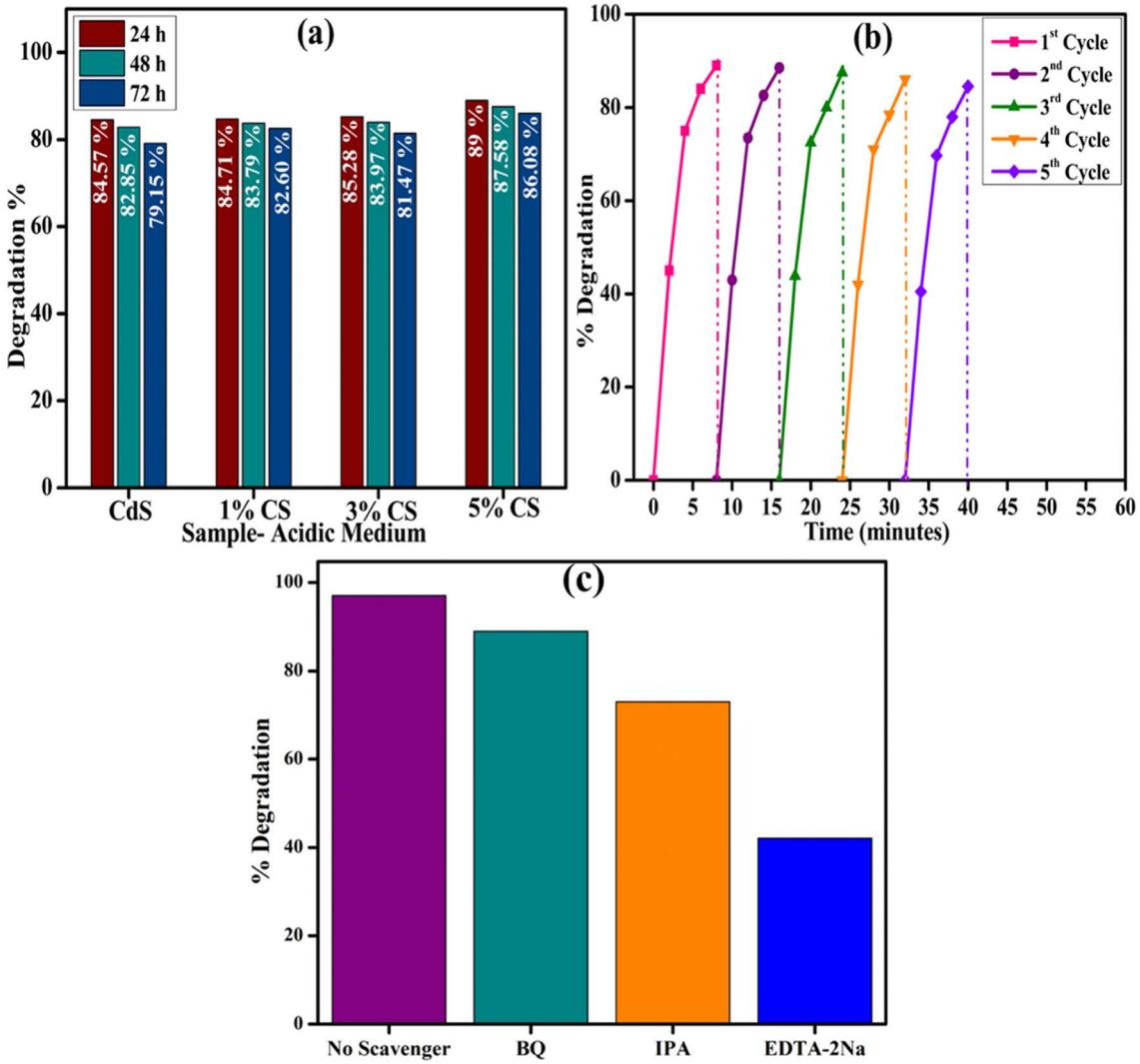

Fig. 10 (a) Stability and (b) reusability of the synthesized nanocatalyst for degradation of RhB dye in an acidic medium; (c) trapping experiment of active species during degradation of RhB.

indicates that H^+ is the predominant active species and significantly influences the degradation process, further supported by the involvement of $^{\bullet}OH$, whereas $^{\bullet}O_2^-$ plays a trivial role in the overall catalysis process.

The antibacterial efficiency of the prepared samples against Gram-negative bacteria (*E. coli*) is summarized in Table 2. The inhibition zone was recorded to between 0–2.85 mm against low dose (500 μg/50 μL) and 0.60–3.50 mm against high dose (1000 μg/50 μL) for pure and 1%, 3%, and 5% CS doped CdS QDs, respectively (Fig. 11a). All concentrations of synthesized samples at low dosage displayed minimal efficacies (Fig. 11b). In addition to this, an inhibition zone of 5.00 mm against ciprofloxacin (the positive control) and 0 mm DIW (the negative control) has been measured. A negligible efficacy was shown by CdS QDs for *E. coli* at low and high doses, respectively, as shown in Fig. 11a and b. The effectiveness and inhibition zone both gradually increased with an increase in the doping concentration. The literature comparison of the present study with previous results is summarized in Table 3.

Table 2 The antibacterial efficiency of the prepared QDs

Samples	500 μg/50 μL	1000 μg/50 μL
CdS	0	0.60
1% CS-CdS	1.65	2.10
3% CS-CdS	2.05	2.45
5% CS-CdS	2.85	3.50
Ciprofloxacin	5.00	5.00
DIW	0	0

The limited impact of cadmium inhibitory actions, which are localized to a single channel of action, contributes to a reduction in CdS effectiveness as an antibacterial agent. Cadmium can pass through cell membranes and take up replicative potential, which ultimately results in antimicrobial action.[58] The key molecular processes by which quantum dots show their antimicrobial activity are the breakdown of cell walls and membranes, the generation of reactive oxygen species (ROS),

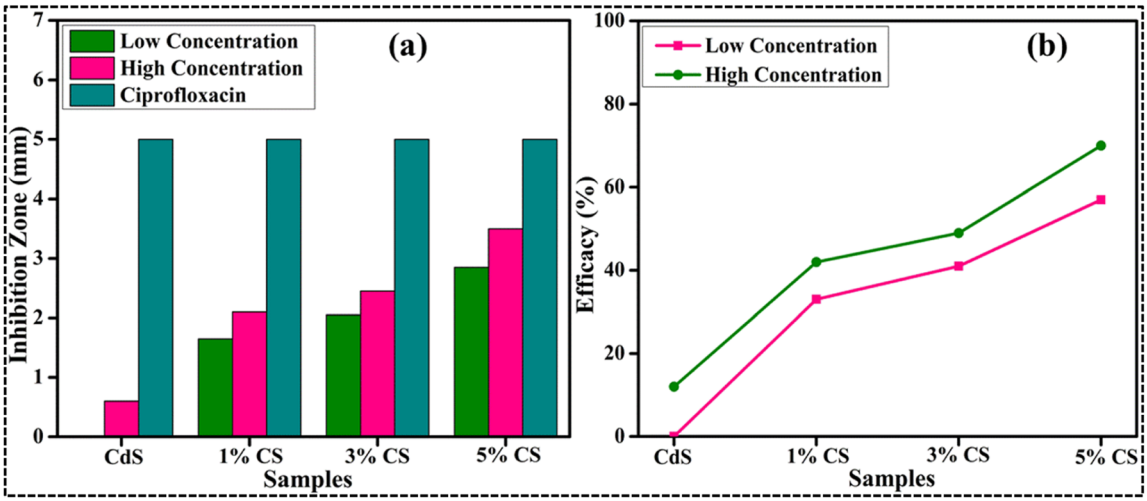

Fig. 11 Graphical representation of antibacterial activity of the *E. coli* pathogen: (a) inhibition zone (mm) and (b) efficacy.

Table 3 Literature comparison study of antibacterial activity with present work

Nanocatalysts	Reduction of the inhibition zone	References
CdS QDs	0.60 mm	2
CdS	0.83 mg ml^{-1}	59
CS/g-C_3N_4/CdS	2.45 mm	60
CdS–Ag_2S	86.4%	61
CdS QDs	22.5%	62
5% CS-CdS	3.50	Present work

and the inhibition of genetic material (DNA/RNA) binding, thereby impeding cell replication. As QD size has an inverse relationship to microbicidal activity, the effectiveness of QDs against microbes also depends on their concentration and diameter. A bacterial burst is caused by the evacuation of cytoplasmic organelles and is caused by the efficient production of ROS by the smaller diameter QDs, which causes bacterial cell membrane breakdown. The electrostatic interaction between cationic Cd^{2+} ions and anionic bacterial membrane components is thought to cause death of harmful bacteria.[2] A possible mechanism of antibacterial activity is demonstrated in Fig. 12.

Extensive research has been conducted on the microbicidal efficacy of nanomaterials containing metal ions and their ability to adhere to bacteria through electrostatic, hydrophobic, or van der Waals forces.[63,64] Potential interactions between formed QDs and residues in active sites for chosen enzyme targets were observed (Fig. 13a and b). These QDs revealed moderate DNA gyrase binding energies and their interaction with indispensable amino acids. Interaction with Ala47, Val71, and Asp73 in docked complexes was observed with binding scores of 1.61 (Fig. 13c and d), implying a role as a DNA gyrase inhibitor.

The binding patterns of the resulting QDs in β-lactamase *E. coli* were almost comparable (Fig. 13b), demonstrating

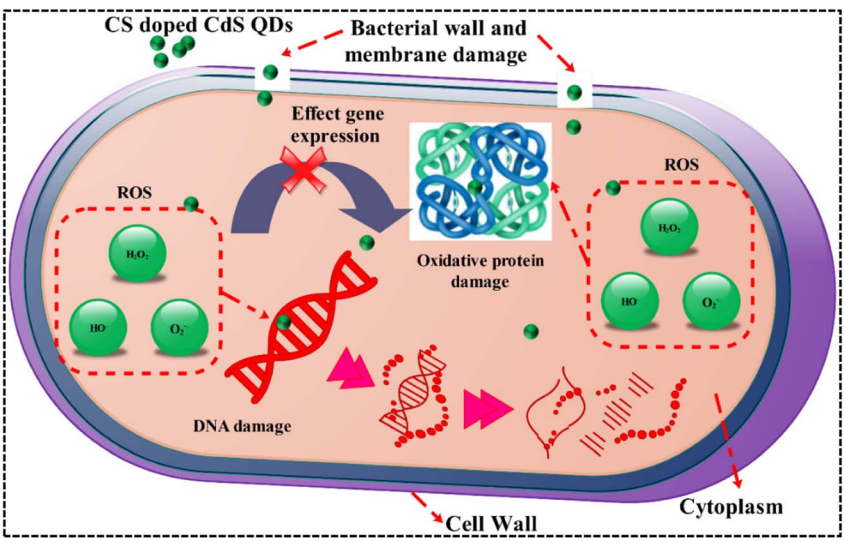

Fig. 12 Proposed mechanism of antibacterial activity.

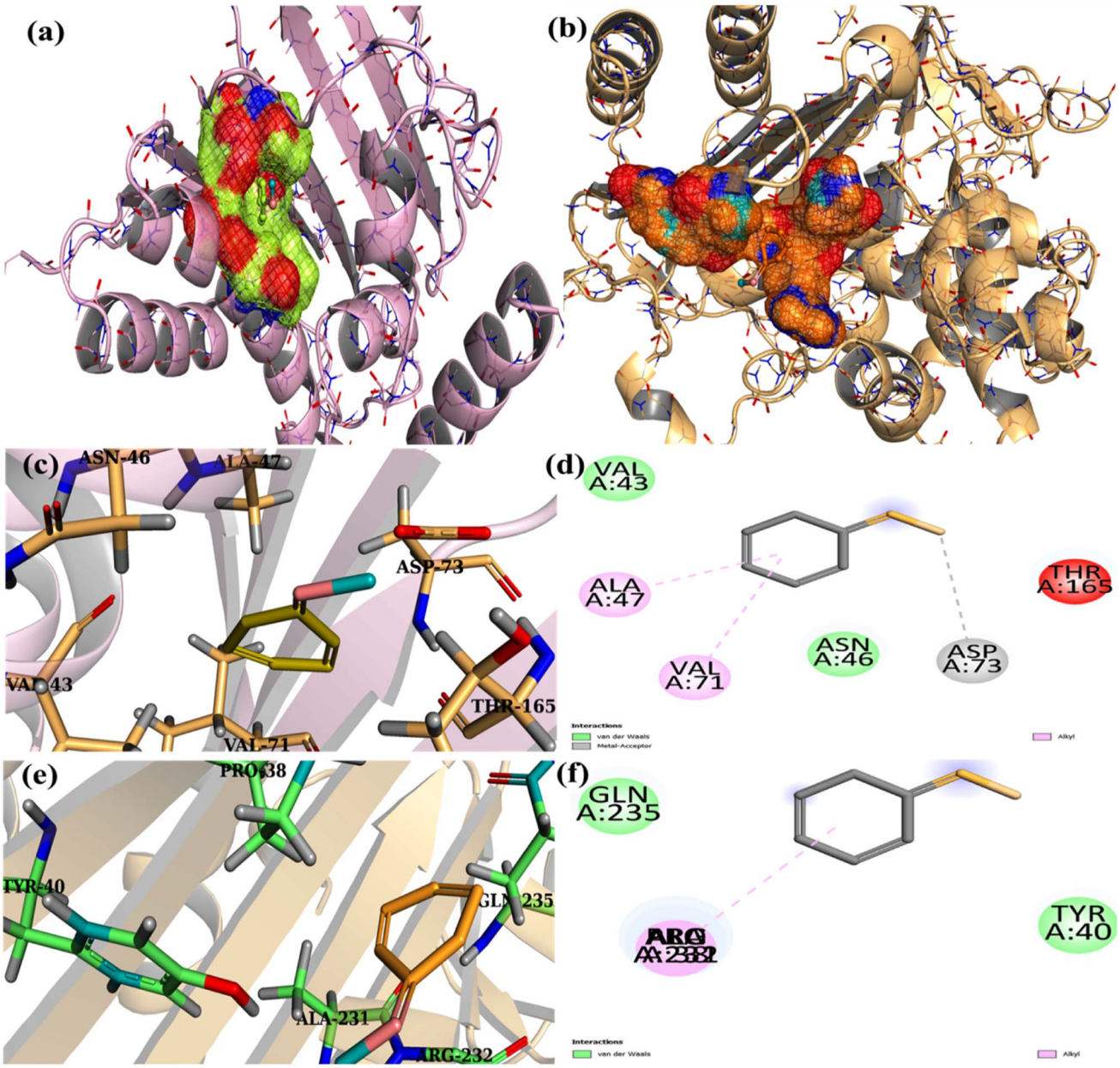

Fig. 13 3D view of binding interaction of QDs within the active site of DNA gyrase *E. coli* (a) and β-lactamase (b). Binding interaction patterns of CS-CdS (c) (3D) and (d) (2D) of DNA gyrase and (e) (3D) and (f) (2D) of CS-CdS inside the active pocket of β-lactamase from *E. coli*.

a superimposed alkyl association with the Arg232, Ala231, and Pro38 amino acids of the active pocket and an overall binding score of 1.84 (Fig. 13e and f).

In silico results are close to *in vitro* bactericidal activity of *E. coli*, and CS-CdS quantum dots have been viewed as potential inhibitors that require further investigation. Moreover, these QDs are proposed to be potential inhibitors of β-lactamase and DNA gyrase enzymes based on *in silico* predictions correlating with antibacterial activities against *E. coli*.

4. Conclusion

The co-precipitation method successfully synthesized different concentrations (1, 3, and 5 wt%) of CS-doped CdS. Several diffraction peaks were observed in the XRD pattern, which confirmed the successful preparation of hexagonal CdS. Moreover, the most intense (002) diffraction plane denoted the preferred formation of CdS crystallites along the [001] direction. Two diffraction peaks of CS were identified at $2\theta = 24.3°$ and 44.0° and an increase in crystallite size was found upon doping. SEM analysis shows that the prepared samples exhibited a non-uniform chunk-like structure with medium-sized particles. The EDS examination revealed the acute and intense peaks of Cd and S, indicating that the product is exceptionally pure. A quantum dot morphology of the CdS was observed, and agglomeration of the particles upon CS doping was shown during TEM analysis, decreasing particle size. A UV-visible spectroscopy study noted a prominent absorption band at

505 nm. Furthermore, 5% CS-doped CdS QDs showed considerable degradation of RhB (89%) in an acidic solution due to morphological changes that occurred after CS doping. Due to the production of ROS, the maximum inhibitory zone against *E. coli* was observed to be 3.5 mm.

Data availability

On-demand, data will be available from the corresponding author.

Conflicts of interest

There are no conflicts to declare.

Acknowledgements

This research was funded by the Princess Nourah bint Abdulrahman University Researchers Supporting Project number (PNURSP2023R7), Princess Nourah bint Abdulrahman University, Riyadh, Saudi Arabia.

References

1 N. Qutub, P. Singh, S. Sabir, S. Sagadevan and W. C. Oh, Enhanced photocatalytic degradation of Acid Blue dye using CdS/TiO_2 nanocomposite, *Sci. Rep.*, 2022, **12**, 1–18, DOI: **10.1038/s41598-022-09479-0**.

2 A. Rafique, M. Ikram, A. Haider, A. Ul-Hamid, S. Naz, W. Nabgan, J. Haider and I. Shahzadi, Dye degradation, antibacterial activity and molecular docking analysis of cellulose/polyvinylpyrrolidone-doped cadmium sulphide quantum dots, *Int. J. Biol. Macromol.*, 2022, **214**, 264–277, DOI: **10.1016/j.ijbiomac.2022.06.058**.

3 W. Fu and W. Zhang, Microwave-enhanced membrane filtration for water treatment, *J. Membr. Sci.*, 2018, **568**, 97–104, DOI: **10.1016/j.memsci.2018.09.064**.

4 K. H. Hama Aziz, H. Miessner, S. Mueller, A. Mahyar, D. Kalass, D. Moeller, I. Khorshid and M. A. M. Rashid, Comparative study on 2,4-dichlorophenoxyacetic acid and 2,4-dichlorophenol removal from aqueous solutions *via* ozonation, photocatalysis and non-thermal plasma using a planar falling film reactor, *J. Hazard. Mater.*, 2018, **343**, 107–115, DOI: **10.1016/j.jhazmat.2017.09.025**.

5 M. Nasrollahzadeh, Z. Issaabadi and S. M. Sajadi, Green synthesis of a Cu/MgO nanocomposite by: Cassytha filiformis L. extract and investigation of its catalytic activity in the reduction of methylene blue, congo red and nitro compounds in aqueous media, *RSC Adv.*, 2018, **8**, 3723–3735, DOI: **10.1039/c7ra13491f**.

6 M. Nasrollahzadeh, M. Sajjadi and S. Mohammad Sajadi, Biosynthesis of copper nanoparticles supported on manganese dioxide nanoparticles using Centella asiatica L. leaf extract for the efficient catalytic reduction of organic dyes and nitroarenes, *Chin. J. Catal.*, 2018, **39**, 109–117, DOI: **10.1016/S1872-2067(17)62915-2**.

7 F. Salimi, S. S. Emami and C. Karami, Removal of methylene blue from water solution by modified nano-boehmite with Bismuth, *Inorg. Nano-Met. Chem.*, 2018, **48**, 31–40, DOI: **10.1080/24701556.2017.1357628**.

8 J. Hassan, M. Ikram, A. Ul-Hamid, M. Imran, M. Aqeel and S. Ali, Application of Chemically Exfoliated Boron Nitride Nanosheets Doped with Co to Remove Organic Pollutants Rapidly from Textile Water, *Nanoscale Res. Lett.*, 2020, **15**, 1–13, DOI: **10.1186/s11671-020-03315-y**.

9 R. Dou, H. Cheng, J. Ma and S. Komarneni, Manganese doped magnetic cobalt ferrite nanoparticles for dye degradation *via* a novel heterogeneous chemical catalysis, *Mater. Chem. Phys.*, 2020, **240**, 122181, DOI: **10.1016/j.matchemphys.2019.122181**.

10 P. L. Ruegg, A 100-Year Review: Mastitis detection, management, and prevention, *J. Dairy Sci.*, 2017, **100**, 10381–10397, DOI: **10.3168/jds.2017-13023**.

11 N. Zaatout, An overview on mastitis-associated Escherichia coli: Pathogenicity, host immunity and the use of alternative therapies, *Microbiol. Res.*, 2022, **256**, 126960, DOI: **10.1016/j.micres.2021.126960**.

12 F. Vangroenweghe, L. Duchateau and C. Burvenich, Short communication: J-5 Escherichia coli vaccination does not influence severity of an Escherichia coli intramammary challenge in primiparous cows, *J. Dairy Sci.*, 2020, **103**, 6692–6697, DOI: **10.3168/jds.2019-17799**.

13 Y. Xie, Y. He, P. L. Irwin, T. Jin and X. Shi, Antibacterial activity and mechanism of action of zinc oxide nanoparticles against Campylobacter jejuni, *Appl. Environ. Microbiol.*, 2011, 77, 2325–2331, DOI: **10.1128/AEM.02149-10**.

14 A. Salem, E. Saion, N. M. Al-Hada, H. Mohamed Kamari, A. H. Shaari, C. A. C. Abdullah and S. Radiman, Synthesis and characterization of CdSe nanoparticles *via* thermal treatment technique, *Results Phys.*, 2017, **7**, 1556–1562, DOI: **10.1016/j.rinp.2017.04.026**.

15 Z. Zheng, M. Mounsamy, N. Lauth-De Viguerie, Y. Coppel, S. Harrisson, M. Destarac, C. Mingotaud, M. L. Kahn and J. D. Marty, Luminescent zinc oxide nanoparticles: From stabilization to slow digestion depending on the nature of polymer coating, *Polym. Chem.*, 2019, **10**, 145–154, DOI: **10.1039/c8py01387j**.

16 V. Beena, S. Ajitha, S. L. Rayar, C. Parvathiraja, K. Kannan and G. Palani, Enhanced Photocatalytic and Antibacterial Activities of ZnSe Nanoparticles, *J. Inorg. Organomet. Polym. Mater.*, 2021, **31**, 4390–4401, DOI: **10.1007/s10904-021-02053-7**.

17 A. Rafiq, M. Imran, M. Aqeel, M. Naz, M. Ikram and S. Ali, Study of Transition Metal Ion Doped CdS Nanoparticles for Removal of Dye from Textile Wastewater, *J. Inorg. Organomet. Polym. Mater.*, 2020, **30**, 1915–1923, DOI: **10.1007/s10904-019-01343-5**.

18 J. Han, F. Dai, Y. Liu, R. Zhao, L. Wang and S. Feng, Synthesis of CdSe/$SrTiO_3$ nanocomposites with enhanced photocatalytic hydrogen production activity, *Appl. Surf. Sci.*, 2019, **467–468**, 1033–1039, DOI: **10.1016/j.apsusc.2018.10.267**.

19 Q. Zhang, Z. Ji, J. Zhou, X. Zhao and X. Lan, Preparation of lanthanum oxide nanoparticles by chemical precipitation

method, *Mater. Sci. Forum*, 2012, 233–236, DOI: 10.4028/www.scientific.net/MSF.724.233.

20 D. Ayodhya and G. Veerabhadram, Facile fabrication, characterization and efficient photocatalytic activity of surfactant free ZnS, CdS and CuS nanoparticles, *J. Sci.: Adv. Mater. Devices*, 2019, **4**, 381–391, DOI: 10.1016/j.jsamd.2019.08.006.

21 R. Arunadevi, M. Latha, S. Velumani, G. Oza, P. Reyes-Figueroa, M. Rohini, I. G. Becerril-Juarez, J. H. Lee and J. Yi, Synthesis and characterization of cadmium sulfide nanoparticles by chemical precipitation method, *J. Nanosci. Nanotechnol.*, 2015, **15**, 8434–8439, DOI: 10.1166/jnn.2015.11472.

22 D. S. R. Josephine, B. Sakthivel, K. Sethuraman and A. Dhakshinamoorthy, Synthesis, Characterization and Catalytic Activity of CdS-Graphene Oxide Nanocomposites, *ChemistrySelect*, 2016, **1**, 2332–2340, DOI: 10.1002/slct.201600384.

23 O. Yamamoto, J. Sawai and T. Sasamoto, Activated carbon sphere with antibacterial characteristics, *Mater. Trans.*, 2002, **43**, 1069–1073, DOI: 10.2320/matertrans.43.1069.

24 S. H. Yoo, J. K. Kang, S. C. Lee, H. Y. Jang and S. B. Kim, Analysis of adsorption characteristics of diclofenac to sucrose-derived carbon spheres from aqueous solutions, *J. Environ. Chem. Eng.*, 2021, **9**, 106573, DOI: 10.1016/j.jece.2021.106573.

25 D. H. Bergey and J. G. Holt, *Bergey's Manual of Determinative Bacteriology*, Williams & Wilkins, Baltimore SE, 9th edn, 1994.

26 A. W. Bauer, W. M. Kirby, J. C. Sherris and M. Turck, Antibiotic susceptibility testing by a standardized single disk method, *Am. J. Clin. Pathol.*, 1966, **45**, 493–496.

27 F. Adzitey, S. Yussif, R. Ayamga, S. Zuberu, F. Addy, G. Adu-Bonsu, N. Huda and R. Kobun, Antimicrobial Susceptibility and Molecular Characterization of Escherichia coli Recovered from Milk and Related Samples, *Microorganisms*, 2022, **10**(7), 1335.

28 M. J. Ferraro, *Performance Standards for Antimicrobial Susceptibility Testing: Eleventh Informational Supplement*, 2020, M100.

29 B. A. Iwalokun, A. Ogunledun, D. O. Ogbolu, S. B. Bamiro and J. Jimi-Omojola, In vitro antimicrobial properties of aqueous garlic extract against multidrug-resistant bacteria and Candida species from Nigeria, *J. Med. Food*, 2004, **7**, 327–333, DOI: 10.1089/jmf.2004.7.327.

30 A. Haider, M. Ijaz, M. Imran, M. Naz, H. Majeed, J. A. Khan, M. M. Ali and M. Ikram, Enhanced bactericidal action and dye degradation of spicy roots' extract-incorporated fine-tuned metal oxide nanoparticles, *Appl. Nanosci.*, 2020, **10**, 1095–1104, DOI: 10.1007/s13204-019-01188-x.

31 A. Haider, M. Ijaz, S. Ali, J. Haider, M. Imran, H. Majeed, I. Shahzadi, M. M. Ali, J. A. Khan and M. Ikram, Green Synthesized Phytochemically (Zingiber officinale and Allium sativum) Reduced Nickel Oxide Nanoparticles Confirmed Bactericidal and Catalytic Potential, *Nanoscale Res. Lett.*, 2020, **15**, 1–11, DOI: 10.1186/s11671-020-3283-5.

32 Ayesha, M. Imran, A. Haider, I. Shahzadi, S. Moeen, A. Ul-Hamid, W. Nabgan, A. Shahzadi, T. Alshahrani and M. Ikram, Polyvinylpyrrolidone and chitosan-coated magnetite (Fe_3O_4) nanoparticles for catalytic and antimicrobial activity with molecular docking analysis, *J. Environ. Chem. Eng.*, 2023, **11**, 110088, DOI: 10.1016/J.JECE.2023.110088.

33 S. Barelier, O. Eidam, I. Fish, J. Hollander, F. Figaroa, R. Nachane, J. J. Irwin, B. K. Shoichet and G. Siegal, Increasing chemical space coverage by combining empirical and computational fragment screens, *ACS Chem. Biol.*, 2014, **9**, 1528–1535, DOI: 10.1021/cb5001636.

34 I. Shahzadi, M. Islam, H. Saeed, A. Haider, A. Shahzadi, J. Haider, N. Ahmed, A. Ul-Hamid, W. Nabgan, M. Ikram and H. A. Rathore, Formation of biocompatible MgO/cellulose grafted hydrogel for efficient bactericidal and controlled release of doxorubicin, *Int. J. Biol. Macromol.*, 2022, **220**, 1277–1286, DOI: 10.1016/j.ijbiomac.2022.08.142.

35 I. Shahzadi, M. Islam, H. Saeed, A. Shahzadi, J. Haider, A. Haider, M. Imran, H. A. Rathore, A. Ul-Hamid, W. Nabgan and M. Ikram, Facile synthesis of copolymerized cellulose grafted hydrogel doped calcium oxide nanocomposites with improved antioxidant activity for anti-arthritic and controlled release of doxorubicin for anti-cancer evaluation, *Int. J. Biol. Macromol.*, 2023, **235**, 123874.

36 A. Bari, M. Ikram, A. Haider, A. Ul-Hamid, J. Haider, I. Shahzadi, G. Nazir, A. Shahzadi, M. Imran and A. Ghaffar, Evaluation of bactericidal potential and catalytic dye degradation of multiple morphology based chitosan/polyvinylpyrrolidone-doped bismuth oxide nanostructures, *Nanoscale Adv.*, 2022, **4**, 2713–2728, DOI: 10.1039/d2na00105e.

37 S. P. Smrithi, N. Kottam, A. Narula, G. M. Madhu, R. Mohammed and R. Agilan, Carbon dots decorated cadmium sulphide heterojunction-nanospheres for the enhanced visible light driven photocatalytic dye degradation and hydrogen generation, *J. Colloid Interface Sci.*, 2022, **627**, 956–968, DOI: 10.1016/j.jcis.2022.07.100.

38 A. Faisal, A. Abadi, A. D. Faisal and A. A. Aljubouri, Synthesis and Production of Carbon Nanospheres Using Noncatalytic CVD Method, *Int. J. Adv. Mater. Res.*, 2016, **2**, 86–91.

39 J. Yu, Y. Yu and B. Cheng, Enhanced visible-light photocatalytic H_2-production performance of multi-armed CdS nanorods, *RSC Adv.*, 2012, **2**, 11829–11835, DOI: 10.1039/c2ra22019a.

40 R. Singh and B. Pal, Fine-tuning the photoluminescence and photocatalytic properties of CdS nanorods of varying dimensions, *Mater. Res. Bull.*, 2013, **48**, 1403–1410, DOI: 10.1016/j.materresbull.2012.12.027.

41 A. Singer, Z. Barakat, S. Mohapatra and S. S. Mohapatra, Nanoscale Drug-Delivery Systems: *In Vitro* and *In Vivo* Characterization, in *Nanocarriers Drug Deliv. Nanosci. Nanotechnol. Drug Deliv.*, Elsevier, 2018, pp. 395–419, DOI: 10.1016/B978-0-12-814033-8.00013-8.

42 F. Henry, P. Marchal, J. Bouillard, A. Vignes, O. Dufaud and L. Perrin, The effect of agglomeration on the emission of particles from nanopowders flow, *Chem. Eng. Trans.*, 2013, **31**, 811–816, DOI: 10.3303/CET1331136.

43 J. Zhang, S. Wageh, A. A. Al-Ghamdi and J. Yu, New understanding on the different photocatalytic activity of wurtzite and zinc-blende CdS, *Appl. Catal., B*, 2016, **192**, 101–107, DOI: **10.1016/j.apcatb.2016.03.058**.

44 N. S. Nirmala Jothi, P. Dennis Christy, A. R. Baby Suganthi, G. Ramalingam and P. Sagayaraj, Development of CdS nanorods of high aspect ratio under hydrothermal conditions with PEG template, *J. Cryst. Growth*, 2011, **316**, 126–131, DOI: **10.1016/j.jcrysgro.2010.12.055**.

45 D. Kandi, A. Behera, S. Martha, B. Naik and K. M. Parida, Quantum confinement chemistry of CdS QDs plus hot electron of Au over TiO_2 nanowire protruding to be encouraging photocatalyst towards nitrophenol conversion and ciprofloxacin degradation, *J. Environ. Chem. Eng.*, 2019, **7**, 102821, DOI: **10.1016/j.jece.2018.102821**.

46 A. S. Berestennikov, Y. Li, I. V. Iorsh, A. A. Zakhidov, A. L. Rogach and S. V. Makarov, Beyond quantum confinement: Excitonic nonlocality in halide perovskite nanoparticles with Mie resonances, *Nanoscale*, 2019, **11**, 6747–6754, DOI: **10.1039/c8nr09837a**.

47 K. Mallick, M. Witcomb and M. Scurrell, Silver nanoparticle catalysed redox reaction: An electron relay effect, *Mater. Chem. Phys.*, 2006, **97**, 283–287, DOI: **10.1016/j.matchemphys.2005.08.011**.

48 S. W. Chook, C. H. Chia, C. H. Chan, S. X. Chin, S. Zakaria, M. S. Sajab and N. M. Huang, A porous aerogel nanocomposite of silver nanoparticles-functionalized cellulose nanofibrils for SERS detection and catalytic degradation of rhodamine B, *RSC Adv.*, 2015, **5**, 88915–88920, DOI: **10.1039/c5ra18806g**.

49 M. Aqeel, M. Rashid, M. Ikram, A. Haider, S. Naz, J. Haider, A. Ul-Hamid and A. Shahzadi, Photocatalytic, dye degradation, and bactericidal behavior of Cu-doped ZnO nanorods and their molecular docking analysis, *Dalton Trans.*, 2020, **49**, 8314–8330, DOI: **10.1039/d0dt01397h**.

50 A. Shahpal, M. Aziz Choudhary and Z. Ahmad, An investigation on the synthesis and catalytic activities of pure and Cu-doped zinc oxide nanoparticles, *Cogent Chem.*, 2017, **3**, 1301241, DOI: **10.1080/23312009.2017.1301241**.

51 M. F. Luo, Y. P. Song, J. Q. Lu, X. Y. Wang and Z. Y. Pu, Identification of CuO species in high surface area CuO-CeO_2 catalysts and their catalytic activities for CO oxidation, *J. Phys. Chem. C*, 2007, **111**, 12686–12692, DOI: **10.1021/jp0733217**.

52 W. Shen, X. Dong, Y. Zhu, H. Chen and J. Shi, Mesoporous CeO_2 and CuO-loaded mesoporous CeO_2: Synthesis, characterization, and CO catalytic oxidation property, *Microporous Mesoporous Mater.*, 2005, **85**, 157–162, DOI: **10.1016/j.micromeso.2005.06.006**.

53 K. A. Adegoke, M. Iqbal, H. Louis and O. S. Bello, Synthesis, characterization and application of CdS/ZnO nanorod heterostructure for the photodegradation of Rhodamine B dye, *Mater. Sci. Energy Technol.*, 2019, **2**, 329–336, DOI: **10.1016/j.mset.2019.02.008**.

54 H. Ullah, E. Viglašová and M. Galamboš, Visible light-driven photocatalytic rhodamine B degradation using CdS nanorods, *Processes*, 2021, **9**, 1–11, DOI: **10.3390/pr9020263**.

55 X. L. Yin, S. R. Han and L. L. Li, CdS@MoS2 core@shell nanorod heterostructures for efficient photocatalytic pollution degradation with good stability, *Optik*, 2020, **220**, 165252, DOI: **10.1016/j.ijleo.2020.165252**.

56 Q. Wang, S. Zhu, S. Zhao, C. Li, R. Wang, D. Cao and G. Liu, Construction of Bi-assisted modified CdS/TiO_2 nanotube arrays with ternary S-scheme heterojunction for photocatalytic wastewater treatment and hydrogen production, *Fuel*, 2022, **322**, 124163, DOI: **10.1016/j.fuel.2022.124163**.

57 N. Qutub, P. Singh, S. Sabir, S. Sagadevan and W. C. Oh, Enhanced photocatalytic degradation of Acid Blue dye using CdS/TiO_2 nanocomposite, *Sci. Rep.*, 2022, **12**, 1–18, DOI: **10.1038/s41598-022-09479-0**.

58 A. M. Mostafa, E. A. Mwafy and M. S. Hasanin, One-pot synthesis of nanostructured CdS, CuS, and SnS by pulsed laser ablation in liquid environment and their antimicrobial activity, *Opt. Laser Technol.*, 2020, **121**, 105824, DOI: **10.1016/j.optlastec.2019.105824**.

59 A. Kumar, S. Singh and D. Kumar, Evaluation of antimicrobial potential of cadmium sulphide nanoparticles against bacterial pathogens, *Int. J. Pharm. Sci. Rev. Res.*, 2014, **24**, 202–207.

60 M. Ikram, H. Maghfoor, A. Shahzadi, A. Haider, I. Shahzadi, N. Abid, A. Ul-Hamid, J. Haider, W. Nabgan and A. R. Butt, Towards effective dye degradation and antimicrobial behavior of chitosan and C_3N_4-doped CdS nanoparticles, *Mater. Today Commun.*, 2022, **33**, 104814, DOI: **10.1016/j.mtcomm.2022.104814**.

61 T. Iqbal, F. Ali, N. R. Khalid, M. B. Tahir and M. Ijaz, Facile synthesis and antimicrobial activity of CdS-Ag_2S nanocomposites, *Bioorg. Chem.*, 2019, **90**, 103064, DOI: **10.1016/j.bioorg.2019.103064**.

62 D. Borah, P. Saikia, P. Sarmah, D. Gogoi, A. Das, J. Rout, N. N. Ghosh, P. Pandey and C. R. Bhattacharjee, Photocatalytic and Antibacterial Activity of Fluorescent CdS Quantum Dots Synthesized Using Aqueous Extract of Cyanobacterium Nostoc carneum, *Bionanoscience*, 2023, **13**, 650–666, DOI: **10.1007/s12668-023-01115-z**.

63 M. Ikram, K. Chaudhary, A. Shahzadi, A. Haider, I. Shahzadi, A. Ul-Hamid, N. Abid, J. Haider, W. Nabgan and A. R. Butt, Chitosan/starch-doped MnO_2 nanocomposite served as dye degradation, bacterial activity, and insilico molecular docking study, *Mater. Today Nano*, 2022, **20**, 100271, DOI: **10.1016/j.mtnano.2022.100271**.

64 M. Ikram, J. Hassan, A. Raza, A. Haider, S. Naz, A. Ul-Hamid, J. Haider, I. Shahzadi, U. Qamar and S. Ali, Photocatalytic and bactericidal properties and molecular docking analysis of TiO_2nanoparticles conjugated with Zr for environmental remediation, *RSC Adv.*, 2020, **10**, 30007–30024, DOI: **10.1039/d0ra05862a**.